External Influences on Hurricane Intensity. Part II: Vertical Structure and Response of the Hurricane Vortex

JOHN MOLINARI AND DAVID VOLLARO

Department of Atmospheric Science, State University of New York at Albany

(Manuscript received 16 August 1989, in final form 20 February 1990)

ABSTRACT

The vertical structure of the interaction of Hurricane Elena (1985) with a baroclinic wave was evaluated using analyses from the European Centre for Medium Range Weather Forecasting. During the period of interaction, azimuthal eddies produced a localized flux convergence of cyclonic angular momentum in the upper troposphere which shifted to progressively smaller radii prior to major secondary deepening of the storm. These momentum fluxes decayed above and below the outflow layer. Eddy heat fluxes showed maximum cooling in the middle and upper troposphere and warming in the lower stratosphere, reflecting the temperature structure of the baroclinic wave as it moved into the hurricane volume.

The response of the hurricane vortex to the fluxes of heat and angular momentum was determined by solution of Eliassen's balanced vortex equation. The balanced solutions showed a band of upward motion, with deep inflow and narrow outflow, which shifted inward from the 500 km radius to the hurricane core in the 24 hours prior to the secondary deepening. The position and timing of this feature corresponded to the contracting outflow maximum found in Part I. Eddy heat fluxes contributed to the induced circulation in the same manner as momentum fluxes near the core, but with smaller magnitude and areal coverage. The contracting outflow maximum thus appeared to represent the upper branch of a secondary circulation excited primarily by the eddy momentum fluxes.

The reintensification of hurricanes is often directly associated with formation of a wind maximum at inner radii which replaces or reinforces the original eye wall as it contracts. Such a feature was seen in reconnaissance data in Elena at the time the secondary circulation reached inner radii. It is speculated that the relatively weak secondary circulation evolved into a local wind maximum through the actions of diabatic heat sources. The approaching trough is thus viewed not as a direct cause of deepening, but as a catalyst which organized the diabatic sources in such a way as to excite internal instabilities of the system.

1. Introduction

In Part I of this work (Molinari and Vollaro 1989a), outflow layer winds in Hurricane Elena were analyzed every 12 hours over the lifetime of the storm using wind data from the international rawinsonde network and from upper level, satellite-derived cloud motion vectors. A high correlation was found between radial fluxes of angular momentum by azimuthal eddies 1500-1800 km from the storm center and pressure changes in the storm core 27–33 hours later. The results supported the view that upper tropospheric angular momentum fluxes can bring about intensity changes in tropical cyclones (Pfeffer and Challa 1981; Holland and Merrill 1984), but the lag in response of the tropical cyclone core had not previously been described. Molinari and Vollaro (1989a; hereafter Part I) proposed that the major secondary deepening of Elena over water, with its preceding "backing in" of an outflow maximum to the storm core, was driven by inward eddy fluxes of cyclonic angular momentum associated with a middle latitude trough that interacted with the storm. It was further proposed that the lag represented an adjustment of the hurricane vortex to the momentum fluxes.

Much of the reasoning above could not be supported by direct evidence because only the outflow layer was analyzed; data at other levels were insufficient for meaningful analysis to be done. As a result, the vertical structure of both the forcing and the radial–vertical circulations which occurred in response could not be determined. In addition, evidence supporting eddy angular momentum fluxes as the forcing for the observed outflow layer divergent flow was circumstantial, and eddy heat flux forcing—which should be nonzero—could not be computed from winds only. It was not clear a priori whether heat fluxes should support or oppose the influence of momentum fluxes.

In the current work, the above issues will be addressed using three-dimensional analyses of both mass and wind from the European Center for Medium Range Weather Forecasting (ECMWF). Although

Corresponding author address: Prof. John E. Molinari, Department of Atmospheric Science, State University of New York at Albany, Earth Science 219, Albany, NY 12222.

these analyses suffer from lack of data as well, the four-dimensional data assimilation process in the ECMWF model should provide additional information in data poor regions. The ECMWF analyses allow calculation of both heat and angular momentum fluxes and their vertical structure. In addition, the balanced vortex equation of Eliassen (1952) will be solved numerically to determine the radial–vertical circulation induced by these fluxes. The results will provide a diagnostic measure of the interaction between the hurricane and the middle latitude wave which will be used to test the hypotheses of Part I.

2. Utility of the ECMWF data

The three-dimensional analyses from ECMWF were obtained on a 2.5° latitude–longitude grid at seven standard pressure levels: 1000, 850, 700, 500, 300, 200, and 100 mb. The ECMWF analyses are constructed using an optimum interpolation method starting from a six hour model forecast, followed by nonlinear normal mode initialization in a form which includes diabatic heating (Wergen 1988).

Inspection of the ECMWF analyses showed that two fundamental requirements were met: (i) with the exception of 0000 UTC 30 August, the location of the storm on the 2.5° latitude–longitude grid, as defined by the maximum midtropospheric relative vorticity, was at the grid point nearest to its true location in nature; and (ii) the maximum vorticity occurred at the same point throughout the lower and middle troposphere, as it must in the mature stages of a hurricane.

Reed et al. (1988) have noted that ECMWF analyses accurately reproduce many aspects of Atlantic easterly waves, including the wave from which Hurricane Elena formed. The authors attributed this success to two major changes in the ECMWF global spectral model in spring of 1985: more sophisticated physics, and the adoption of the high resolution T106 truncation. Heckley et al. (1987) showed using the Betts (1986) cumulus parameterization that the complex track of Elena was well forecast by ECMWF starting from 1200 UTC 31 August, which was shown in Part I to be a key time in the momentum flux forcing. The results of the above studies suggest that the initial analyses more than adequately represent the three-dimensional structure of the hurricane environment.

The ECMWF analyses were interpolated bilinearly in the horizontal and linearly in pressure to the same cylindrical grids as in Part I, with Δr = 100 km, $\Delta\lambda$ = 15°, and Δp = 100 mb. The analyses will be compared in this section to those of Part I at 200 mb, the only level at which they overlap. The previous analyses will be taken as "truth", because they made use of extensive upper tropospheric cloud motion vectors and because they showed many subtle features of the interaction between the hurricane and the middle latitude trough.

As in Part I, all calculations were done in a Lagrangian coordinate following the storm. Storm-relative velocity components were computed by subtracting the 12-hour average storm motion from the total velocity.

Figures 1–3 show radius–time (r–t) sections of 200 mb azimuthal mean tangential velocity $\bar{v}$, mean radial velocity $\bar{u}$, and eddy angular momentum flux, for both the Part I objective analyses and the ECMWF analyses.

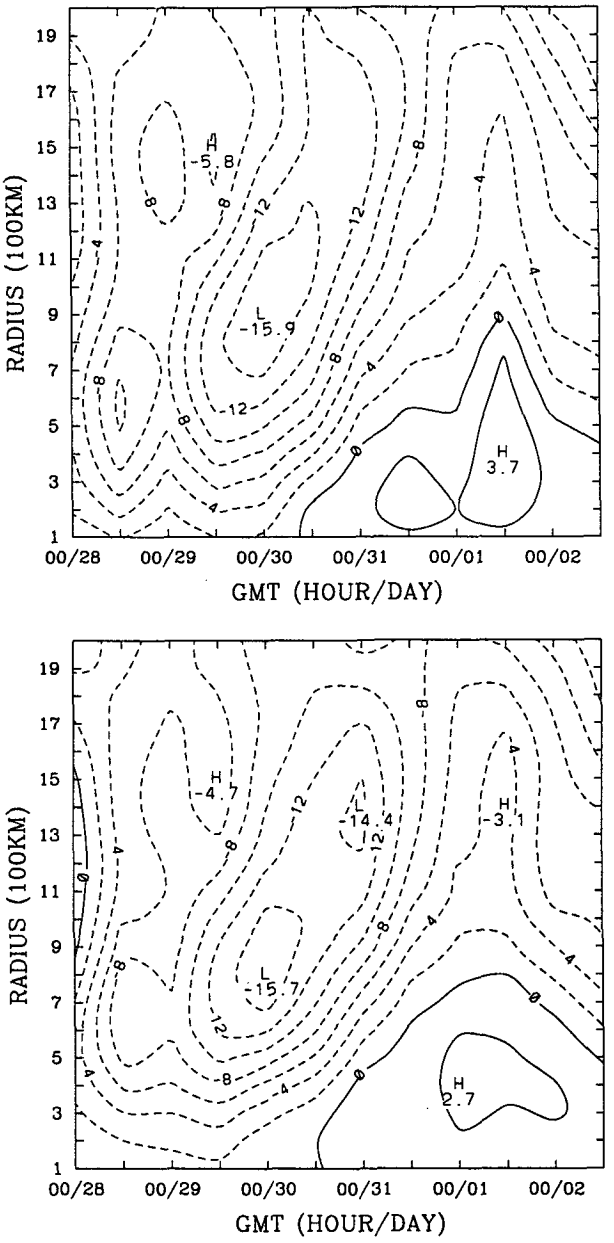

FIG. 1. (a) Radius–time series of azimuthally averaged tangential velocity, as determined from the outflow layer (200 mb) objective wind analyses of Molinari and Vollaro (1989a). Negative values are represented by dashed contours. The contour increment is 2 m s^{-1}; (b) Same as (a), but derived from the ECMWF analyses interpolated to the same cylindrical grid.

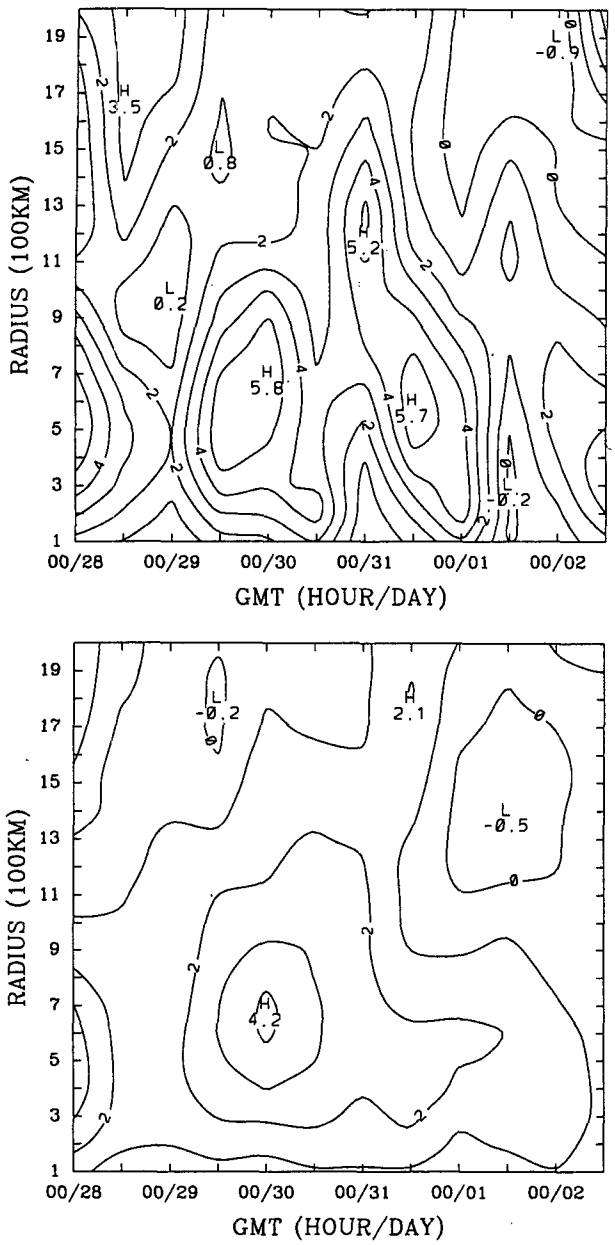

FIG. 2. Same as Fig. 1, but for azimuthally averaged radial velocity. Contour increment 1 m s^{-1}.

The rms differences in $\bar{v}$ and $\bar{u}$ between the two analyses were 1.2 and 1.5 m s^{-1}, respectively, surprisingly small given the entirely different procedures for preparing the analyses (the point by point rms differences in u and v were 4.0 and 3.6 m s^{-1}, respectively). Although the $\bar{u}$ and $\bar{v}$ differences were of the same order, the percentage difference was smaller in the mean tangential velocity, which was typically twice the magnitude of the radial velocity. In addition, Figs. 1 and 2 show that the tangential velocity gradient strongly resembled that in Part I, while the radial velocity gradient differed significantly. Lee et al. (1989) found similar problems in FGGE IIIb data from 1979.

The global model initialization procedure likely plays the major role in the differences between the Part I and ECMWF-derived winds. The $\bar{v}$ field in a hurricane is primarily rotational, while $\bar{u}$ is primarily divergent. Normal mode initialization without heating suppresses unbalanced divergent flow. The added diabatic component of the ECMWF initialization is determined by fixing the mean heating from a two hour forecast of

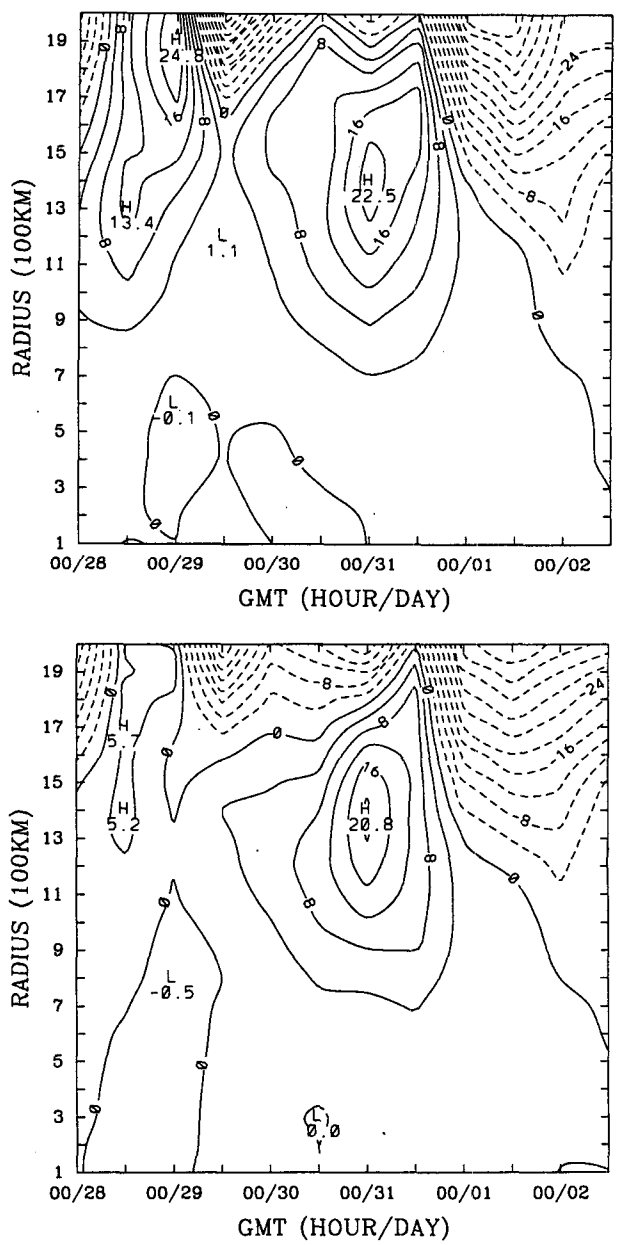

FIG. 3. Same as Fig. 1, but for radial flux of relative angular momentum by azimuthal eddies, given by Eq. (1). Contour increment 4×10^{17} kg m^2 s^{-2}.

the model during the normal mode initialization process (Wergen 1988). Thus heating-induced divergence is present only to the extent that the model has generated a realistic field of heating in two hours. Because all models have difficulties with spinup of precipitation fields, the initialized divergence field is likely to be underestimated. Hollingsworth et al. (1989) have found such an underestimate of lower and upper level divergence in the ECMWF tropical analyses. This weakness is most apparent in the Elena analyses at 1200 UTC 29 August, eight hours after the storm moved from land to water and rapidly intensified: in the Part I analysis, outflow quickly grew from 2 to 5 m s^{-1} at the 400 km radius (Fig. 2a), while in the ECMWF analysis, outflow increased only to 2.5 m s^{-1} at the same radius (Fig. 2b). Only after 12 additional hours, when the outflow had presumably come closer to a balanced state, did the ECMWF outflow reach 4 m s^{-1}. Later, on 31 August, the inward shift of the outflow maximum during the period of enhanced eddy momentum flux, which appeared to play a major role in the secondary deepening, was not captured by the ECMWF analyses. As a result, the mean radial velocity from the ECMWF analyses appears to be inadequate for verifying the radial–vertical circulations proposed in Part I.

Figure 3 shows 200 mb eddy momentum flux, which has been assumed (for display purposes) to be valid over a 200 mb thick layer to allow direct comparison with Part I. This flux is given (Holland 1983) by

$$-\frac{2\pi r^2}{g}\int_p \overline{u'_L v'_L}\,dp \qquad (1)$$

where the primes indicate the deviation from the azimuthal mean and the subscript L represents storm relative flow. As noted by Holland (1983), $\bar{u}_L = \bar{u}$ and $\bar{v}_L = \bar{v}$, so that differences between the Lagrangian and Eulerian coordinate systems arise only in nonlinear advective terms.

The eddy momentum fluxes in Fig. 3, which involve products of deviations from the $\bar{u}$ and $\bar{v}$ fields, were similar in the two analyses, even though the $\bar{u}$ field differed. This paradox arises due to two factors. First, the largest eddy wind components, and the largest localized $u'_L v'_L$, occurred north of the storm within the United States rawinsonde network, where the ECMWF analysis should be most accurate. Because $|u'_L| \gg |\bar{u}|$ north of the storm, the eddy fluxes still had the correct sign and approximately correct magnitude, despite the 1.5 m s^{-1} rms differences in $\bar{u}$. Second, eddies during the period of interaction with the trough primarily represent the trough itself (Molinari and Vollaro 1989a). The eddies are thus part of the balanced, largely rotational flow which should be well represented in the analyzed fields. These two circumstances do not exist in all storms, and it is not certain whether eddy angular momentum fluxes from ECMWF analyses would always be as realistic as in this study.

The above results arose from interpolating the ECMWF analyses to cylindrical grids centered on the observed positions of the storm. Because storm positions on the 2.5° grid invariably differed from those observed simply due to the coarseness of the grid, the fields in Fig. 1–3 were reinterpolated to cylindrical grids centered on the ECMWF analyzed storm center positions. The resulting rms difference in $\bar{u}$ remained 1.5 m s^{-1}, but difference in $\bar{v}$ rose to 1.8 m s^{-1}. Although the inward propagating outflow maximum appeared marginally in the reinterpolated $\bar{u}$ field, the overall structure remained substantially different from that in Fig. 2a. This difference, plus the larger anomalies in the reinterpolated $\bar{v}$, indicate that use of the observed center locations in Figs. 1–3 was not responsible for the differences between ECMWF and our previous analyses.

One obvious limitation of the 2.5° latitude–longitude analysis is lack of resolution. Figure 4 shows a pressure–time series of mean tangential velocity at 700 mb. The maximum speed occurs near the 300 km radius, and inner core details are absent. Nevertheless, the radius of maximum winds is constant in the vertical and in time, avoiding spurious oscillations in intensity and position sometimes seen in earlier data sets (Merrill, personal communication 1989). In addition, time variations in ECMWF derived maximum tangential wind in Fig. 4 correspond reasonably well to reconnaissance aircraft derived central pressure fluctuations shown in Fig. 8. It will later be shown (section 4f) that the large radius of maximum winds does not adversely influence the calculated response to large scale forcing.

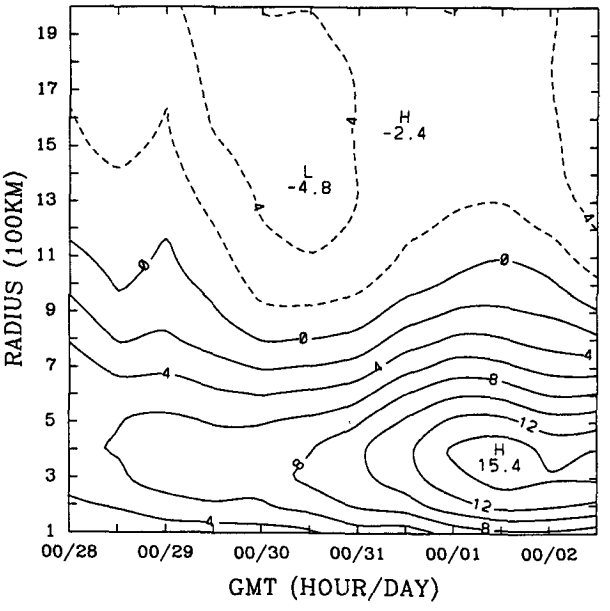

FIG. 4. Radius–time section of 700 mb mean tangential velocity; otherwise as in Fig. 1(b).

Overall, the ECMWF analyses produced realistic outflow layer $\bar{v}$ and $u'_L v'_L$ fields outside the storm core, but inadequate $\bar{u}$ fields. It will be assumed that these conditions hold in the lower and middle troposphere as well, where no alternate detailed analyses exist for comparison. Thus, the ECMWF $\bar{u}$ fields will not be discussed; instead, $\bar{u}$ will be computed from the balanced vortex solution discussed in section 4.

3. Hurricane structure

a. Radial-vertical cross sections

Figure 5 shows vertical cross sections of the radial convergence of eddy flux of tangential velocity [m s^{-1} day^{-1}; first right-hand side term of Eq. (6) in the following section] at two critical times on 31 August. The spinup by azimuthal eddies reached a maximum in the outflow layer and decreased rapidly above and below, consistent with previous results using composited data (McBride and Zehr 1981; as shown by Pfeffer and Challa 1981). In this individual case, however, the flux convergence shifted inward with time, with upper tropospheric values exceeding 25 m s^{-1} day^{-1} within 500 km of the center on 1200 UTC 31 August. Subsequent to that time, eddy flux convergence (not shown) became much weaker and more diffuse, as can be seen indirectly in Fig. 3. As noted in Part I, this momentum flux variation was produced almost entirely by eddies associated with the approach of a middle latitude trough.

The radial convergence of eddy heat flux [first right-hand side term of Eq. (7)] is shown in Fig. 6 at 1200 UTC 31 August, the time of its largest contribution. Cooling by eddies of up to 5 K day^{-1} occurred at middle and upper tropospheric levels, reflecting the movement of a cold trough into the hurricane volume. Because the tropopause was relatively low in the middle latitude trough, the trough represented a warm anomaly at 100 mb, and up to 8 K day^{-1} warming by eddy heat fluxes occurred at that level as the trough approached the hurricane. The zero line of the heat fluxes in the upper troposphere generally coincided with the level of maximum eddy angular momentum flux. The vertical eddy fluxes of both heat and momentum were generally much smaller than the lateral eddy fluxes.

Figure 7 shows a pressure–time section at the 500 km radius of the time rate of change of the mean tangential velocity, as determined from the ECMWF analyses. This figure shows only the 60 hour period prior to and just after the secondary deepening of the storm. Upper levels began to spin up late on 29 August, consistent with the start of significant eddy momentum fluxes shown in Fig. 3 at outer radii and the corresponding large flux convergence at r = 500 km (see Fig. 7 from Part I). Upper level eddy momentum flux convergence dramatically increased during 31 August (Fig. 5), yet by 0600 UTC on that day maximum cyclonic spinup had shifted to middle levels (Fig. 7). This occurred because the upper level momentum source was offset by enhanced outflow (and its associated anticyclonic Coriolis torque), which shifted inward almost exactly in phase with the momentum source (compare Figs. 2a and 5). The maximum spinup did not reach low levels until late on the 31st, well after the onset of upper tropospheric forcing.

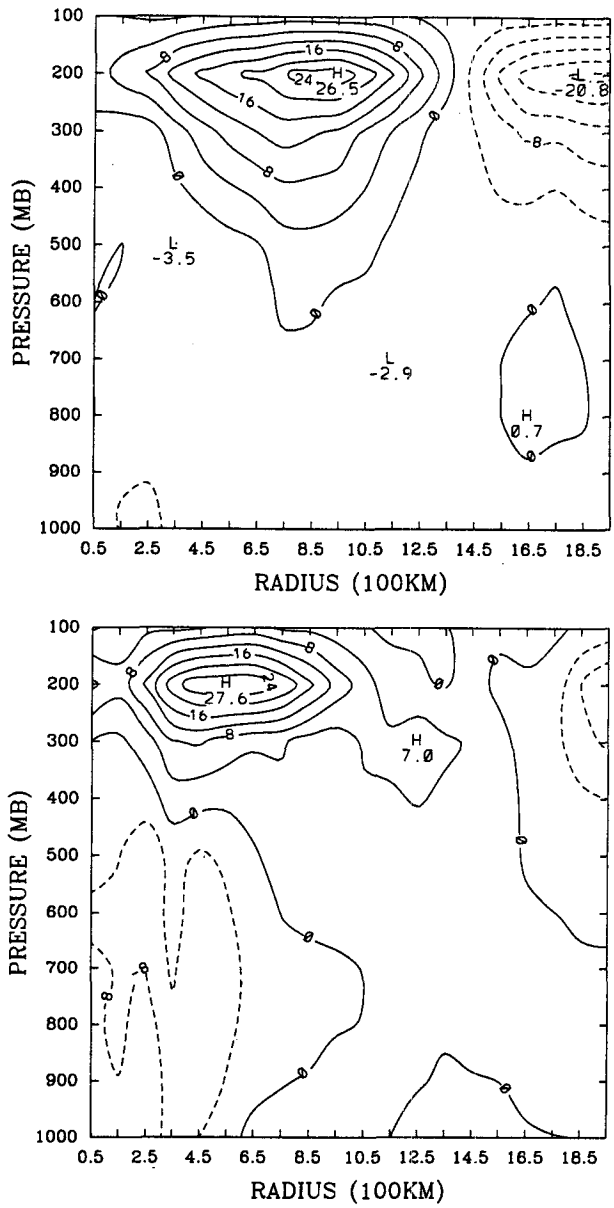

FIG. 5. Radial–vertical cross section of eddy flux convergence of relative angular momentum, divided by r [first right-hand side term in Eq. (6)] for (a) 0000 UTC 31 August; and (b) 1200 UTC 31 August. Negative contours are dashed. Increment: 4 m s^{-1} day^{-1}.

In summary, the observations show that eddy fluxes of angular momentum and heat were substantial in the 36 hours prior to the major secondary deepening of

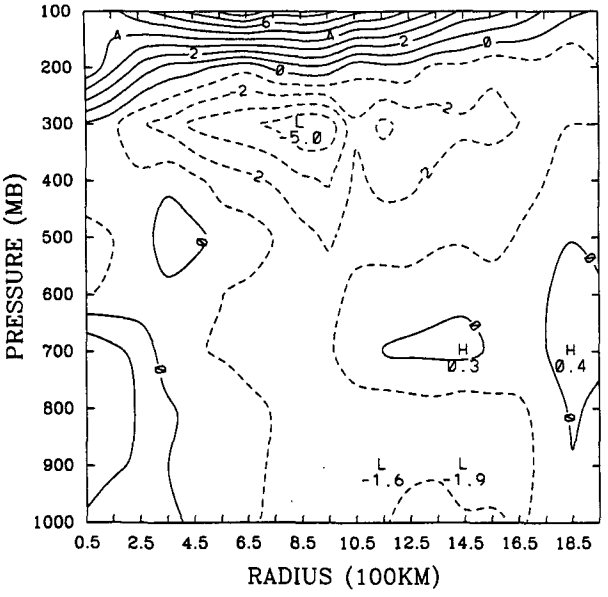

FIG. 6. Radial–vertical cross section of the lateral convergence of eddy heat flux [first right-hand side term of Eq. (7)] at 1200 UTC 31 August. Negative contours are dashed. Increment: 1 K day^{-1}.

Elena as a middle latitude trough approached from the northwest. An outflow maximum developed, apparently in response to upper level momentum flux convergence, and the observed spinup shifted from upper levels to middle and lower levels with time. The vertical structure of the radial velocity could not be determined adequately from the ECMWF analyses and will be calculated diagnostically. The interrelationship between radial–vertical circulation, heat and momentum fluxes, and intensity change in Elena will be investigated in section 4 using balanced vortex solutions.

b. Inner core structure

Previous studies of tropical cyclones (Shapiro and Willoughby 1982; Willoughby et al. 1982, 1984; Willoughby 1989) have shown that a large fraction of intensity changes are preceded by changes in eye wall radius or by formation of a secondary wind maximum outside the eye wall which propagates inward and often supercedes the original eye wall. During the initial contraction of the secondary wind maximum, the storm usually begins to fill but eventually deepens again, sometimes to greater intensity than before, as the secondary wind maximum shifts inward and becomes the primary eye wall. Willoughby (1988), in a review of dynamics of the tropical cyclone core, noted that evolution of these convective rings is largely dependent upon internal processes, but the means of formation of such rings remains unresolved.

The inner core structure of Elena has been measured by Willoughby (1989) using aircraft reconnaissance data. Figure 8 shows the times in which three secondary wind maxima occurred, superimposed on the time variation of minimum central pressure (an incomplete fourth secondary maximum just prior to landfall is not shown). None of the three fit the classic behavior described by Willoughby et al. (1982). The first was diffuse and asymmetric, and neither it nor the third were preceded by a period of filling or slow deepening. Both occurred during rapid deepening and did not dramatically extend the period of deepening. The second event is shown in terms of its six-hourly tangential velocity change in Fig. 9 [adapted from data of Willoughby (1989)]. It formed at or outside of the 120 km radius between 0000 and 1200 UTC 31 August and propagated into the storm core late on the same day. Only this second wind maximum significantly influenced the pressure field. Pressure fell slowly during its inward propagation, then fell rapidly for an extended period after it reached the innermost radii. Although the radial profile of wind speed was rather flat at the time this second pulse reached the core, it was during the pressure fall initiated by this feature that a more classical sharpened wind profile developed for the first time in Elena.

It is concluded from the data of Willoughby (1989) that although none of the three secondary wind maxima fit the classic model, the second strongly influenced the evolution of the storm. The possibility of external forcing of this event will be the focus in subsequent calculations.

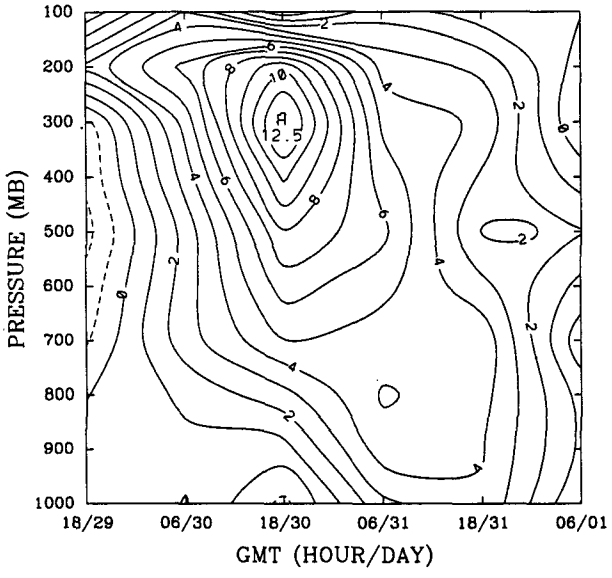

FIG. 7. Pressure–time series of the time rate of change of the azimuthally averaged tangential velocity at the 500 km radius. Values are for 12 hour periods centered on the times shown on the abscissa. Negative contours are dashed. Only a 60 hour subset prior to and during the major secondary intensification of Hurricane Elena is shown. Increment: 1 m s^{-1} day^{-1}.

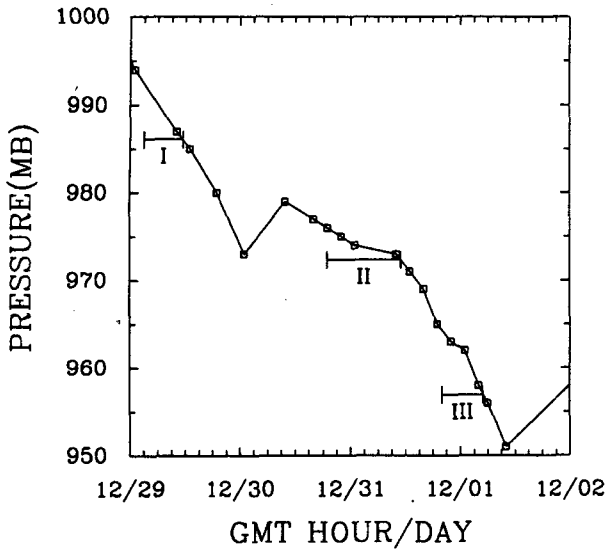

FIG. 8. Time variation of minimum central pressure in Elena with occurrences of secondary wind maxima superimposed. The horizontal lines indicate the period during which each secondary wind maximum was propagating inward toward the center. Secondary wind maximum I shifted from the 140 km to 70 km radius; II shifted from the 120 km radius to the storm core; and III shifted from the 30 km radius to the core. Adapted from data of Willoughby (1989).

4. Balanced vortex solutions

The balanced vortex equation follows Eliassen (1952), but uses storm-relative coordinates and includes eddy heat fluxes on the right-hand side:

$$A\psi_{pp} + 2B\psi_{rp} + C\psi_{rr} - \frac{4B}{r}\psi_p - \left(\frac{1-\kappa}{p}B + \frac{C}{r}\right)\psi_r = r\frac{\partial}{\partial p}\left\{\left(\frac{2\bar{v}_L}{r}+f\right)\left(\frac{\partial \bar{v}_L}{\partial t}\right)_{\text{eddy}}\right\} + \frac{r\pi R}{p}\frac{\partial}{\partial r}\left(\frac{\partial \bar{\theta}}{\partial t}\right)_{\text{eddy}} \quad (2)$$

where ψ subscripts represent partial derivatives, and

$$A = \left(f + \frac{2\bar{v}_L}{r}\right)\left(f + \frac{\partial \bar{v}_L}{\partial r} + \frac{\bar{v}_L}{r}\right) \quad (3)$$

$$B = -\left(f + \frac{2\bar{v}_L}{r}\right)\frac{\partial \bar{v}_L}{\partial p} \quad (4)$$

$$C = -\frac{R\pi}{p}\frac{\partial \bar{\theta}}{\partial p} \quad (5)$$

$$\left(\frac{\partial \bar{v}_L}{\partial t}\right)_{\text{eddy}} = -\frac{1}{r^2}\frac{\partial}{\partial r}r^2\overline{u'_L v'_L} - \frac{\partial}{\partial p}\overline{\omega' v'_L} - \overline{f'u'} \quad (6)$$

$$\left(\frac{\partial \bar{\theta}}{\partial t}\right)_{\text{eddy}} = -\frac{1}{r}\frac{\partial}{\partial r}r\overline{\theta' u'_L} - \frac{\partial}{\partial p}\overline{\theta'\omega'} \quad (7)$$

$$\pi = \left(\frac{p}{p_0}\right)^{R/c_p}. \quad (8)$$

In the derivation of Eq. (2), the storm-relative coordinate alters the advective terms contained within $d\bar{v}/dt$ and $d\bar{\theta}/dt$ (Holland 1983; Skubis and Molinari 1987). Because the d/dt operator is independent of the coordinate system, the right-hand sides of the momentum and thermodynamic equations are uninfluenced by the Lagrangian transformation. Thus the $-\overline{f'u'}$ term in Eq. (6) contains total and not storm-relative velocity.

The left-hand side of (2) has been written in the form given by Sundqvist (1970), which minimizes the number of terms with derivatives in order to reduce truncation error. Eq. (6) and (7) represent the lateral and vertical eddy flux convergence of absolute angular momentum and potential temperature, respectively, which provide the forcing for the hurricane vortex in this study. The radial–vertical circulation induced by the forcing is given by

$$\bar{u} = \frac{1}{r}\frac{\partial \psi}{\partial p} \quad (9)$$

$$\bar{\omega} = -\frac{1}{r}\frac{\partial \psi}{\partial r}. \quad (10)$$

The effects of diabatic heating and friction, both of which are large, have not been included in the balanced vortex equation for reasons which will be discussed below.

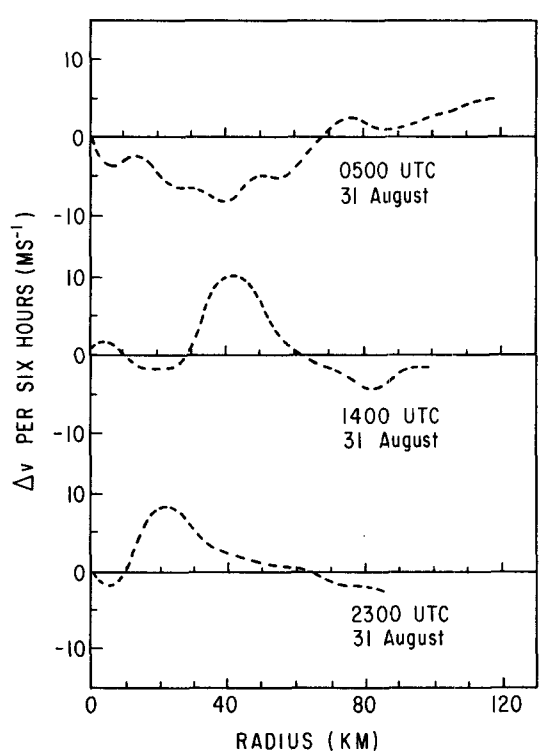

FIG. 9. Six-hourly changes in azimuthally averaged tangential velocity (m s^{-1}) centered on the times shown, indicating the inward shift of secondary wind maximum II.

a. Numerical considerations

Equation (2) was solved by successive overrelaxation over a region which extended radially to 2000 km and vertically from 1000 to 75 mb. Centered differencing was used for all derivatives. The radial grid spacing was 25 km and the vertical spacing 25 mb, even though the input data had only 250 km and 100 mb resolution. This excess resolution, similar to that of Holland and Merrill (1984), was adopted to reduce truncation error during the relaxation. Despite the high resolution, the inner structure of the hurricane contains only information interpolated from the much coarser resolution analyses.

Following Sundqvist (1970), the streamfunction was set to zero at $r = 0$ and at the top and bottom, which implies $\bar{u} = 0$ at $r = 0$, and $\bar{\omega} = 0$ at 1000 mb and 75 mb. At $r = 2000$ km, $\partial\psi/\partial r = 0$, consistent with $\bar{\omega} = 0$ at the outer boundary. The calculated $\bar{\omega}$ could have been used to define the streamfunction gradient at the outer boundary, but its value is small. Using zero instead gives homogeneous boundary conditions on all sides, which allows the contributions of each forcing function to be determined independently without ambiguity.

Although localized regions of negative absolute vorticity occurred in the outflow layer, the ellipticity condition ($B^2 - AC < 0$) was always met in the azimuthally averaged fields. Other numerical aspects of the solution of (2) are discussed in the Appendix.

b. Limitations of the balanced vortex calculation

As noted above, diabatic heating and friction have been omitted from the forcing function in (2). Both processes contribute most strongly within 150 km of the center. The initial 2.5° latitude–longitude analysis resolves only the outer edge of the region with Rossby number greater than unity (see Fig. 4), and contains no inner region information. The result is that realistic heating and friction contributions cannot be determined from the ECMWF analyses. Inner core diabatic heating could be incorporated in some idealized manner on the 25 km grid spacing, but in order to determine a realistic response using Eq. (2), the following would have to be known: (i) wind and temperature at inner radii, which are largely unmeasured in this storm except at the 850 mb aircraft reconnaissance flight level; (ii) the vertical distribution of heating, which greatly influences the radial–vertical circulation induced by the heating; and (iii) the location of heating with respect to the radius of maximum wind, which also influences the response at inner radii (Schubert and Hack 1982). Similar arguments hold for the inclusion of friction. The addition of heating and friction would make the solutions of (2) largely dependent on the somewhat arbitrary choices of inner core structure.

Instead the responses were computed only to the resolvable eddy heat and momentum fluxes provided by the ECMWF analyses. Although the solution to (2) frames the problem as forcing by the eddies and response of the vortex, the forcing in reality goes in both directions; i.e., the fluxes themselves are likely to be shaped in part by processes in the vortex core. Nevertheless, such diagnostic calculations have proven useful in studying idealized tropical cyclones (Shapiro and Willoughby 1982; Smith 1981; Schubert and Hack 1982) and composited observed tropical cyclones (Pfeffer and Challa 1981; Holland and Merrill 1984). Three major issues will be addressed by the balanced vortex solutions: (i) determination of the radial–vertical circulation induced by eddy heat and momentum fluxes, which cannnot be measured by available observations; (ii) the role of such fluxes in the inward propagation of the outflow maximum seen prior to secondary intensification of the storm; and (iii) relative importance of eddy heat fluxes, which have not previously been examined in tropical cyclones.

c. Results

The radial–vertical circulation determined from Eq. (2) falls into fairly distinct regimes during the life cycle of Elena. Fig. 10 shows the streamfunction and associated $\bar{u}$ and $\bar{\omega}$ with all right-hand side forcing terms included, averaged over the first three periods ending 0000 UTC 29 August. In this prehurricane stage, the instantaneous circulation induced by processes other than heating and friction was in–up–out, but over a broad region characteristic of a synoptic-scale easterly wave. The scale of the circulation resembles that shown by Molinari and Skubis (1985) during the early stages of Hurricane Agnes of 1972. In the 24 hours after Elena crossed from Cuba to the Gulf of Mexico, the induced upward motion region narrowed, but still extended to the 1000 km radius, with maximum upward motion well outside the core. At the time of formation of secondary wind maximum I (see Fig. 8), upward motion existed at inner radii. Although this provides a favorable environment for such formation, the uncertainty of eddy flux magnitudes at inner radii (Molinari and Vollaro 1989a) does not allow any definite inferences to be drawn.

Figure 11 shows the streamfunction and associated $\bar{u}$ and $\bar{\omega}$ at 1200 UTC 30 August. As the middle latitude trough approached and heat and angular momentum fluxes increased, the response became much more focused. Inflow was primarily outside of the 500 km radius and through a deep layer from near the surface to the midtroposphere, and outflow was in a narrow layer around the 200 mb level. The resultant $\bar{\omega}$ field shows a relatively weak maximum of about 0.5 μbar s^{-1} at the 450 mb level and 450 km radius, well outside of the eye wall. Weak subsidence was present throughout the troposphere outside the 1500 km radius. Because ψ, $\bar{u}$, and $\bar{\omega}$ are directly related, only $\bar{\omega}$ will be shown for subsequent times.

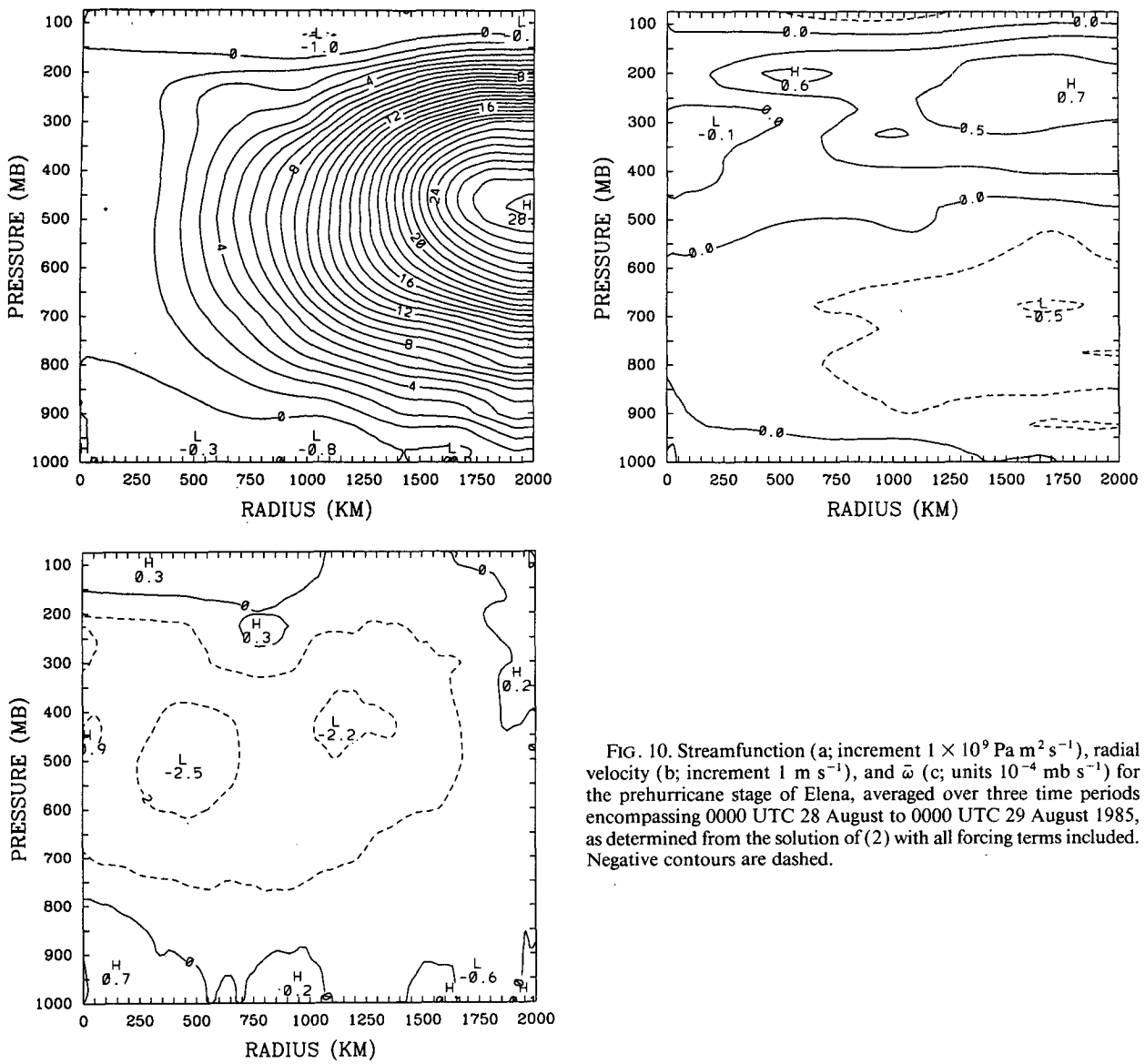

FIG. 10. Streamfunction (a; increment 1×10^9 Pa m^2 s^{-1}), radial velocity (b; increment 1 m s^{-1}), and $\bar{\omega}$ (c; units 10^{-4} mb s^{-1}) for the prehurricane stage of Elena, averaged over three time periods encompassing 0000 UTC 28 August to 0000 UTC 29 August 1985, as determined from the solution of (2) with all forcing terms included. Negative contours are dashed.

Figure 12 shows $\bar{\omega}$ at 0000 UTC 31 August. The upward motion maximum shifted to inside the 300 km radius and intensified by nearly 40% from 12 hours before. Inflow continued through a deep layer while maximum outflow (not shown) intensified to 1.6 m s^{-1} and also shifted inward. Subsidence shifted inward and intensified as well, with tropospheric-deep subsidence occurring from the 1100 to 1800 km radius.

At 1200 UTC 31 August, the upward motion maximum reached the hurricane core region (Fig. 13) and intensified further. It should be emphasized that this balanced circulation does not include heating or frictional effects; the upward motion at the innermost radii in Fig. 13 was associated solely with eddy heat and momentum fluxes. The outflow maximum at this time reached 1.8 m s^{-1} at 200 mb. The maximum subsidence shifted inward to about the 900 km radius, and the subsidence field was broken up into deep but narrow cells, rather than the relatively uniform subsidence of the previous time.

Figures 11–13 show that the azimuthal eddies excited a radial–vertical circulation which shifted inward with time from about the 500 km radius to the center over 24 hours as the middle latitude trough approached Elena. Figure 14 shows an r–t plot of the 200 mb $\bar{u}$ derived from the balanced vortex calculations. The rapid increase in outflow accompanying the initial development of Elena as it reached water between 0000 and 1200 29 August is largely absent. This indicates that the initial deepening was driven by local diabatic processes and not by eddy fluxes outside the storm core. The only significant balanced outflow driven by heat

and momentum fluxes appeared at the 1000 km radius at 0000 UTC 31 August and propagated inward to the 500 km radius 12 hours later. Although the magnitude was less than that observed (Fig. 2) because frictional and diabatic heating effects were not included, the timing and location of the "backing in" of the mean outflow was reproduced. The increased outflow near the center at 0000 UTC 1 September does not appear in the balanced vortex solution. This latter outflow may have been caused by enhanced convection within 100 km of the core which occurred in association with the secondary wind maximum; i.e., it was part of the response to the eddy fluxes.

During the brief existence of secondary wind maximum III (Fig. 8), the balanced $\bar{\omega}$ (Fig. 15) was again upward at inner radii. During the later filling stages of Elena prior to landfall, subsidence occurred in response to the eddies.

In summary, eddies associated primarily with the middle latitude trough drove a favorable in–up–out circulation which propagated inward with time and reached the inner radii simultaneous with the development of secondary maximum II, which preceded the major secondary intensification of Elena. The timing and positioning of the inward propagation of the outflow maximum seen in the observed fields was reproduced in the balanced $\bar{u}$ independent of heating and friction, suggesting that this feature represented a response to the eddy fluxes. The evidence supports the view that interaction of the trough and the hurricane was the external cause of the secondary deepening of Elena. This forcing was indirect, however, in that the

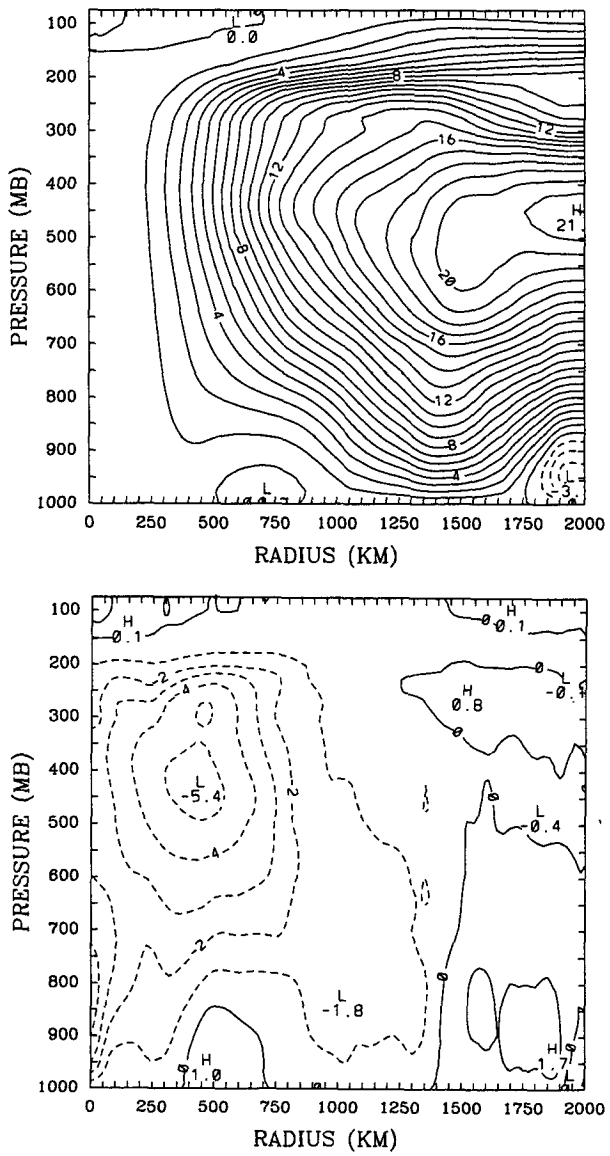

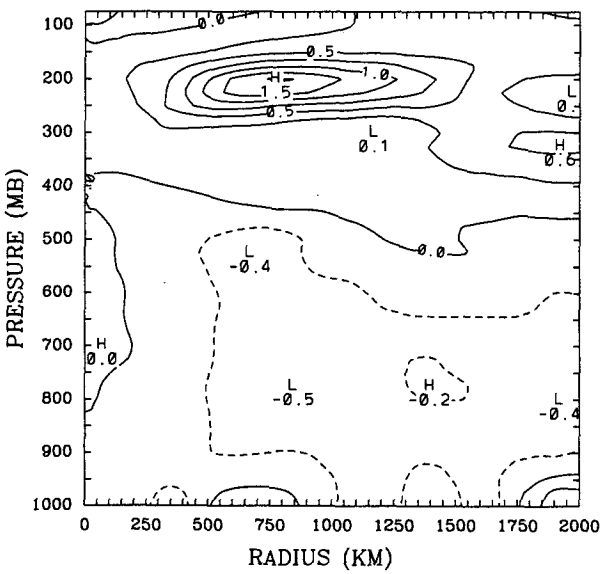

FIG. 11. As in Fig. 10, but for 1200 UTC 30 August 1985.

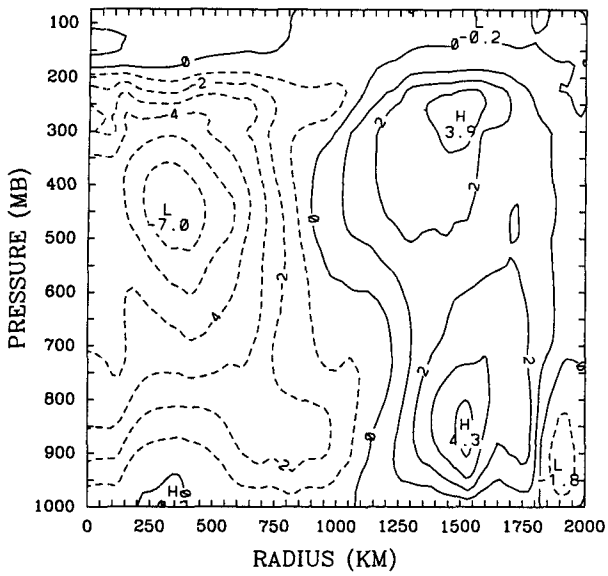

FIG. 12. Balanced vortex $\bar{\omega}$ with all forcing terms included at 0000 UTC 31 August. Units: 10^{-4} mb s^{-1}.

last 22 mb of central pressure fall (Fig. 8) occurred only after the secondary wind maximum associated with the external processes reached the storm core.

d. *Heat flux effects*

Figures 16 and 17 show the balanced $\bar{\omega}$ produced only by the total heat flux convergence at 0000 and 1200 UTC 31 August. Comparison with Fig. 12–13 shows that the maximum contribution to upward motion occurred at the same radii as for the total forcing, but often with less than 20% of the magnitude and with smaller areal coverage. To the extent this is true in other storms, it would account for why momentum fluxes alone correlate well with deepening of tropical cyclones; it is not that heat fluxes play no role, but simply that they may contribute in the same direction as eddy momentum fluxes, at least within 500 km of the storm center.

Comparison of the total induced $\bar{\omega}$ and that due to heat fluxes alone shows that strong heat flux divergence is responsible for the subsidence at middle and outer radii. This likely reflects a response to cold advection as the middle latitude trough propagated into the hurricane volume at middle and outer radii.

e. *Beta effect*

The $\overline{f'u'}$ term in (6) represents the effects of nonzero flow across the circulation in the meridional direction. In the presence of a uniform north to south flow, cyclonic Coriolis torque to the north exceeds anticyclonic torque to the south due to the beta effect, and the storm spins up. Figure 18 shows a representative cross section of $-\overline{f'u'}$ (in m s^{-1} day^{-1} of cyclonic spinup) at 0000 UTC 31 August. Although the magnitude of $\overline{f'u'}$ varied in time, its vertical gradient was remarkably constant: a stronger north to south flow existed at upper levels than in the lower troposphere, producing a large cyclonic eddy momentum source aloft and a small source or sink near the surface. This momentum source variation favors an in–up–out circulation to restore balance, much like the eddy source of relative angular momentum shown in Fig. 5. Because the response was so similar throughout the life cycle of Elena, a time-mean streamfunction was computed by simple averaging of the 12 time periods, and is shown with its associated $\bar{\omega}$ in Fig. 19. Even though the forcing was largest at the outermost radii, the response in $\bar{\omega}$ extended all the way to the storm core. The associated $\bar{u}$ (not shown) contained a 0.3 m s^{-1} inflow maximum at r = 1500 km and p = 800 mb, and a 0.7 m s^{-1} outflow maximum at 1750 km and 200 mb. This effect alone produced a small but steady spinup of the vortex.

The induced circulation requires a vertical gradient of $-\overline{f'u'}$ [see Eqs. (2) and (6)] and thus a vertical shear of the basic current. During the first half of the life cycle of Elena, the upper level flow-through was associated primarily with an outflow jet to the south, and later was maintained by inflow from the north associated with the middle latitude trough. The continuous favorable character of the circulation could be coincidence, or could reflect some influence of the storm on the vertical shear of its environment in order to optimize chances for development. No such mechanism is known, and the reason for the remarkable regularity of the response to $\overline{f'u'}$ during all phases of Elena remains uncertain.

f. *Mean versus eddy contributions*

Schubert and Hack (1982) have noted the large influence of the inertial stability distribution on inner

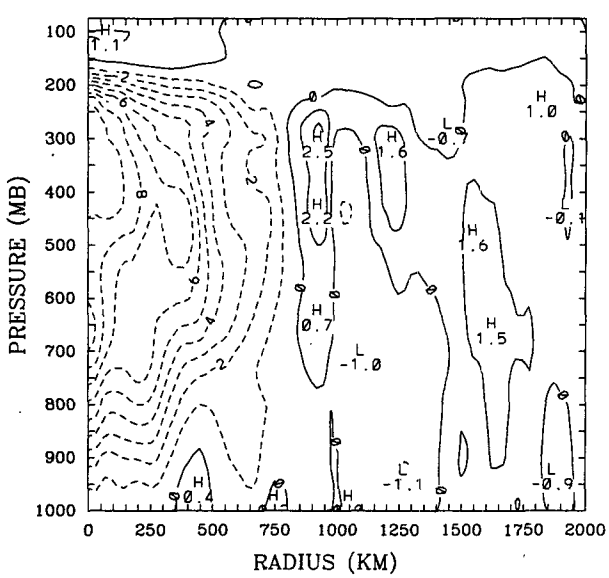

FIG. 13. As in Fig. 12, but for 1200 UTC 31 August.

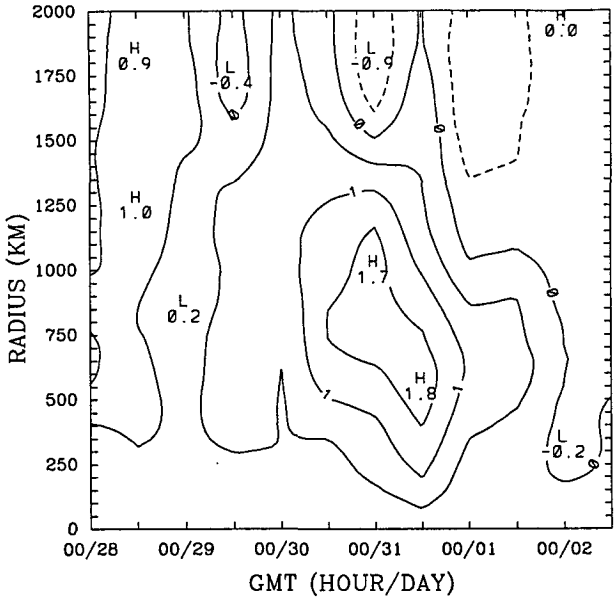

FIG. 14. Radius–time series of 200 mb mean radial velocity from the balanced vortex calculations with all forcing terms included. Increment: 0.5 m s^{-1}.

core circulations in tropical cyclones. Because the radius of maximum winds in the ECMWF data was 300–400 km, the inertial stability distribution differed significantly from that in nature. To test the impact of this resolution problem, the hurricane was removed from the azimuthal mean by setting $\bar{v} = 0$ and $\bar{\theta} = \bar{\theta}(z)$ only, while retaining the eddy terms. As a result, the left-hand side of (2) had the coefficient A containing inertial stability due to f alone, B (baroclinicity effects) equal to 0, and C (vertical stability term) replaced with its area-averaged value at each level. Because $A > 0$ and $C > 0$, the ellipticity condition remained satisfied.

The resulting solutions of (2) were surprisingly similar to their original values. At each radius, $\bar{\omega}$ differences were normalized by the vertically averaged $\bar{\omega}$ magnitude, and this quantity was averaged over all radii. The resulting fractional difference in $\bar{\omega}$ was 14% averaged over all times, with a standard deviation in time of only 4%. The pattern of $\bar{\omega}$ was identical, with maxima and minima at the same radii and pressure levels. Thus, on the scale of the input data, the influence of eddies dominated that of the mean inertial stability and baroclinicity. Within the innermost core of tropical cyclones, of course, this does not hold, as shown by the formal scaling of Shapiro and Willoughby (1982). Nevertheless, it can be concluded that the large radius of maximum winds in the input data does not distort the calculated response.

An additional sensitivity experiment was done by repeating the solution without the mean vortex, but with stability $\partial\theta/\partial p$ replaced by its vertically averaged value. In effect, this procedure slightly increased stability through most of the troposphere, and sharply decreased stability in the lower stratosphere. The resulting $\bar{\omega}$ values differed by 51% ± 7% from the control. The solutions were thus much more sensitive to the vertical variation of stability than to inertial or baroclinic effects. Nevertheless, the resulting pattern of $\bar{\omega}$ still resembled its control value. Figure 20 shows $\bar{\omega}$ for 0000 UTC 31 August, which should be compared to Fig. 12. Despite a 48% normalized $\bar{\omega}$ difference at this hour, the results showing an in–up–out circulation centered at the 350 km radius and 450 mb pressure are qualitatively identical to the control.

Overall, the balanced vortex solutions were relatively insensitive to the mean hurricane structure throughout the life cycle of the storm. Because Elena had no higher a ratio of eddy to mean fluxes than typical tropical cyclones (Molinari and Vollaro 1989a), this result may be of general relevance.

5. Discussion

The calculation of fluxes of heat and angular momentum by azimuthal eddies provides a useful diagnostic framework for examining interactions of tropical cyclones with their environment. Calculation of balanced vortex responses to these fluxes can show when the tropical cyclone core is being influenced by events hundreds of km away, as has been noted by Holland and Merrill (1984). These tools may ultimately provide a means of predicting tropical cyclone intensity change, for which few objective models currently exist.

Because upper tropospheric forcing may take many forms (Gray 1979; Merrill 1988; Lee et al. 1989), more

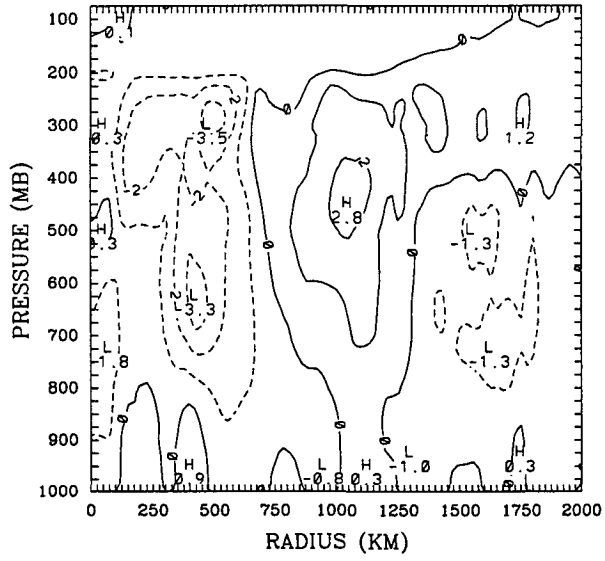

FIG. 15. As in Fig. 12, but for 1200 UTC 1 September 1985.

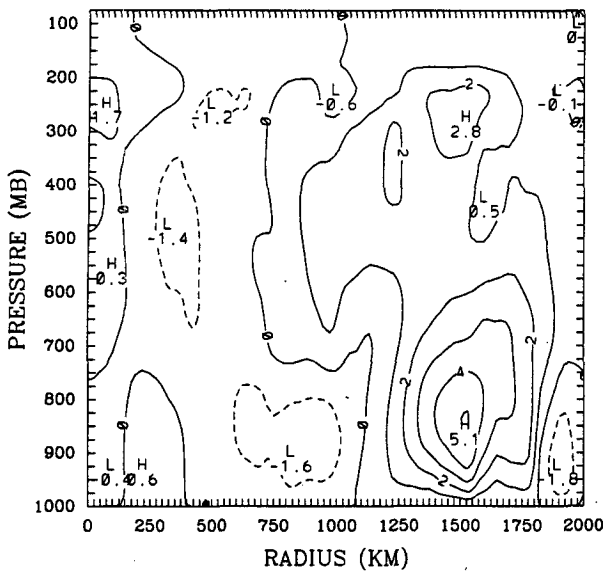

FIG. 16. Balanced vortex $\bar{\omega}$ with lateral and vertical heat flux convergence only at 0000 UTC 31 August. Units: 10^{-4} mb s^{-1}.

case studies will be required to determine how commonly the inward propagating eddy angular momentum source in Hurricane Elena occurs. Gray (personal communication 1989) has found that intensifying tropical cyclones often spin up first in the upper troposphere. Gray attributes this to the influence of vertical momentum transports by enhanced convection, but it may also represent upper tropospheric eddy angular momentum fluxes. McBride and Zehr (1981) found that larger and more organized inward cyclonic momentum fluxes occur in intensifying than nonintensifying tropical cyclones, and Pfeffer and Challa (1981) showed that such fluxes will produce intensification where it would otherwise not occur. These studies, plus the frequent finding that the approach of troughs often precedes deepening of tropical cyclones (see discussion in Molinari and Vollaro 1989a), support the importance of eddy momentum fluxes in tropical cyclone intensification.

The ability to calculate eddy fluxes of momentum and heat in future case studies depends greatly on the accuracy of the input analyses. In this study, the ECMWF analyses appeared to produce accurate estimates of eddy fluxes, but for reasons that may be peculiar to the case study (see section 3). The major uncertainty lies with the divergent flow, primarily the radial flow in tropical cyclones. This weakness may be reduced in recently available high resolution, uninitialized analyses from ECMWF.

a. External forcing versus interaction

It is tempting to label the balanced circulation induced by eddy fluxes as "externally forced", but the work of Ooyama (1987) suggests caution is needed in using this interpretation. With a quiescent environment, Ooyama's shallow water model of the outflow layer forced by fixed mass and momentum sources at the tropical cyclone center produced nearly symmetric anticyclonic flow. When sheared zonal flow was added to the environment, outflow jets—and thus eddy momentum fluxes—developed. Because these fluxes did not occur when environmental flow was absent, they can be thought of as forced by the environment. Without the tropical cyclone, however, the eddy fluxes also would not have occurred. The fluxes must be interpreted as arising from interaction between the storm and its environment and not a simple forcing in one direction or the other.

The Elena case is more complex than that of Ooyama in that the trough would propagate through the hurricane volume regardless of whether the hurricane was present. It is likely, however, that the distribution of eddy fluxes is shaped, as in Ooyama's results, by interactions with the hurricane outflow. Indirect evidence supports this view. When the cylindrical grid was displaced 300 km from the hurricane center in each of four directions, the eddy flux distribution changed significantly in both magnitude and timing, and sometimes even in sign. Substantial changes in eddy fluxes over this small fraction of the middle latitude cyclone wavelength indicate heuristically that interactions on a scale much smaller than that of the synoptic scale trough strongly shaped the flux distribution. This suggests that the eddy fluxes have a mesoscale structure which arises via *interaction* of the hurricane with the trough, rather than a synoptic scale structure caused simply by *propagation* of the trough. The balanced vortex framework is thus limited in that,

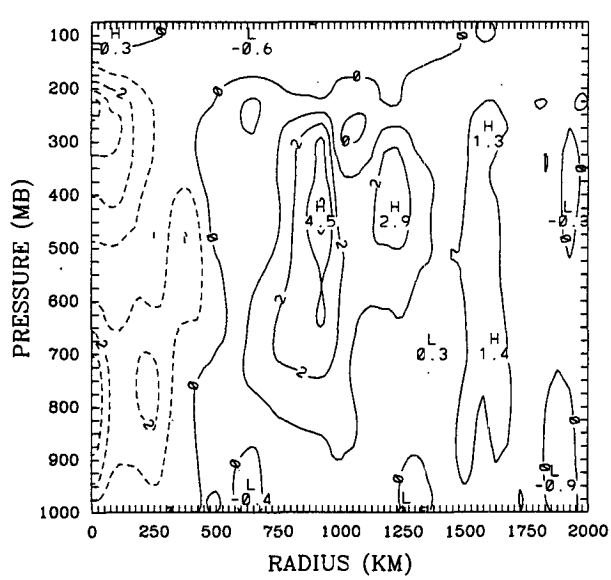

FIG. 17. As in Fig. 16, but for 1200 UTC 31 August.

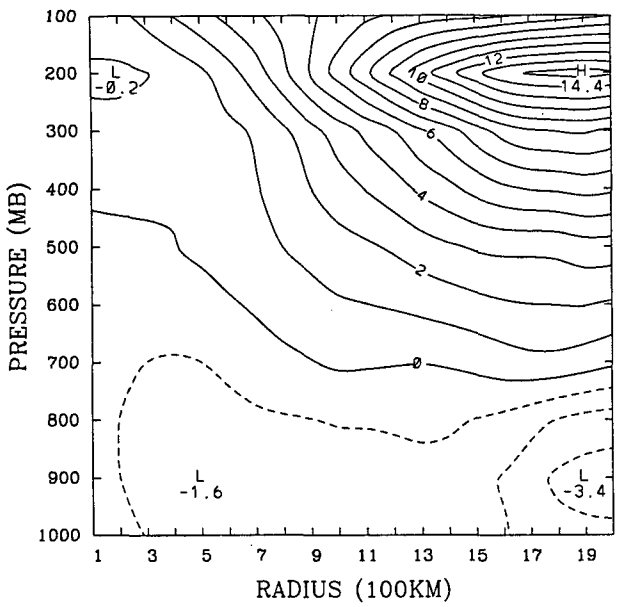

FIG. 18. Radial–vertical cross section of $-\overline{f'u'}$ at 0000 UTC 31 August. Increment: 1 m s^{-1} day^{-1}.

like any diagnostic calculation, it can only show one direction of interaction.

With the above limitation in mind, the balanced vortex solutions proved to be meaningful. They showed that the inward shift of the outflow maximum which preceded major deepening of the hurricane was shaped primarily by eddy angular momentum fluxes, while widespread subsidence at middle and outer radii was associated with heat fluxes. The vertical circulation excited by the eddy fluxes was centered nearly 500 km from the center 36 hours prior to the secondary intensification of Elena, then shifted inward with time, accompanied by deep inflow and narrow upper tropospheric outflow.

Because the effects of eddy angular momentum fluxes dominated those of heat fluxes over the inner 800 km of the storm, the inward propagating updraft can be interpreted as part of the adjustment of the vortex to the momentum fluxes. Upper tropospheric spinup initially creates imbalances: the tangential wind becomes supergradient at 200 mb and the vertical shear in the upper troposphere becomes unbalanced, with cyclonic shear too weak for the given warm core (or the warm core too strong for the given shear). The secondary circulation required to restore balance must do some or all of the following: reduce the spinup at 200 mb by enhancing outflow and corresponding anticyclonic Coriolis torque; spin up middle levels by enhanced inflow; and cool the core region with upward motion. The in–up–out circulation shown by the balanced $\bar{\omega}$ accomplishes all three. Shapiro and Willoughby (1982) showed that eddy momentum sources near the core drive surface pressure falls and thus low-level spinup as well. Although inner core details cannot be seen in the current study, the observed $\partial\bar{v}/\partial t$ at the 500 km radius is qualitatively just as would be expected (Fig. 7): a shift of maximum spinup from upper to middle to lower levels over 24 hours.

Although the initial behavior of the band of upward motion can be attributed to adiabatic adjustment of the vortex to momentum sources, a fundamental change likely occurred at inner radii. Figures 8 and 9 show that a secondary wind maximum appeared at the 120 km radius during the same 12 hour period that the upward motion maximum passed. This provides strong (albeit circumstantial) support for the view that the secondary wind maximum was excited by the interaction of the hurricane with the trough. Because the circulation induced by the eddy fluxes reached only 1 μbar s^{-1}, the development of the wind maximum must have involved some feedback between the convection, local surface fluxes, and the induced circulation. It is speculated that (i) enhanced convection was excited by the band of upward motion, in the radial region that remains unstable outside the convectively neutral core (Ooyama 1982); (ii) this convection produced localized pressure falls and acceleration of the wind; (iii) enhanced surface fluxes allowed further convection as the upward motion maximum moved inward; and (iv) at some inner radius, the response became focused enough by latent heating to be seen as a localized secondary wind maximum. This latter feature then proceeded inward largely independent of its initial forcing, in the manner described by Shapiro and Willoughby (1982), and produced rapid pressure falls as it reached the innermost radii (Fig. 8). Nearly half of the 30-hour

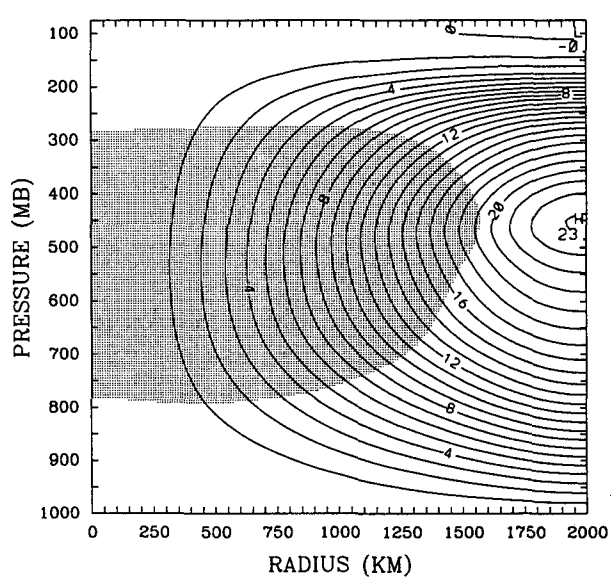

FIG. 19. Time averaged streamfunction (contours, increment 1 $\times$ 10^9 Pa m^2 s^{-1}) from 0000 UTC 28 August to 1200 UTC 2 September, due to the $\overline{f'u'}$ term only, overlaid by the associated $\bar{\omega}$, shaded for values less than -1×10^{-4} mb s^{-1}.

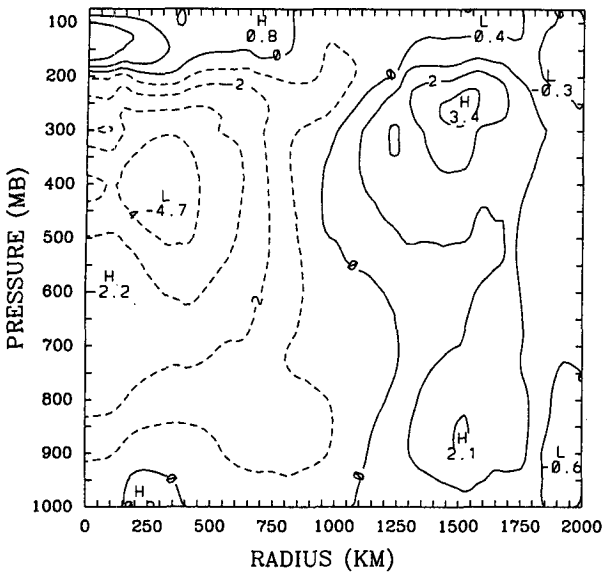

FIG. 20. Balanced $\bar{\omega}$ on 0000 UTC 31 August with all forcing terms included, but with the mean vortex removed and stability $\partial\theta/\partial p$ replaced at all points with its vertical average. Otherwise like Fig. 12, with which it should be compared.

lag between momentum sources and intensification observed in Part I could be attributed to the slow evolution of this latter process.

It is thus proposed that, unlike the initial intensification of Hurricane Elena as it moved from land to water, which likely was produced by internal instabilities, the reintensification of Elena involved two physical mechanisms. First, the interaction of the hurricane with the approaching middle latitude trough produced inward cyclonic momentum fluxes at progressively smaller radii and a localized band of upward motion. Subsequently, the induced circulation organized diabatic sources in such a way as to excite an internal instability of the system. The latter could still be regarded as an air–sea interaction instability (Emanuel 1986; Rotunno and Emanuel 1987), but one less direct than the initial intensification of Elena, in that locally enhanced surface fluxes and associated convection supported the formation of a contracting secondary eye wall.

b. *Future work*

The actual process by which the inward propagating band of upward motion might have excited the secondary eye wall could only be speculated on in this work. Such interactions are difficult to study because they often occur between 50 and 200 km from the storm center, outside or on the edge of reconnaissance aircraft coverage but too close to the storm for conventional data sources. A great need exists for a multilayer data set within 200 km of the hurricane core. This data gap is now being addressed by the dropwindsonde program of the Hurricane Research Division of NOAA (Burpee et al. 1984; Lord and Franklin 1987). Although such instruments cannot for practical reasons sample the outflow layer, they potentially will provide an otherwise three-dimensional description of the development of a secondary eye wall from an externally forced circulation. It is thus conceivable that the interaction between tropical cyclones and their environment at some "critical radius" where the response is focused (Holland 1988; Molinari and Vollaro 1989a) may be observable in coming years.

Larger scale dynamics in this case study are also not fully understood. The balanced vortex approach averages out the azimuthal dimension and frames the problem as one of forcing and response. A complete understanding requires a three-dimensional, time dependent description of the two interacting features. Two approaches are being pursued: evolution of isentropic potential vorticity (Hoskins et al. 1985; see also Molinari and Vollaro 1989b), which expresses the problem in terms of a quasi-conserved variable in three dimensions; and three-dimensional mesoscale numerical modeling, which produces a dynamically balanced dataset that bypasses some of the difficulties with observed data. The results of these studies will be reported at a later time.

Acknowledgements. We thank Lloyd Shapiro of the Hurricane Research Division of NOAA for his critical review of the manuscript, and Hugh Willoughby of HRD/NOAA for providing the inner core data used in section 3. We appreciate the review of Robert Merrill, which helped us to produce a more clearly focused discussion of the intensification process. The gridded analyses used for the balanced vortex solutions were obtained from the European Center for Medium Range Weather Forecasting. This study was supported by NOAA Grants 50-WNCR-8-06055 and 50-WNCR-9-06080.

APPENDIX

Numerical Considerations in the Balanced Vortex Equation Solution

The iteration equation for the solution of Eq. (2) can be written

$$\psi_{ijk}^{m+1} = \psi_{ijk}^{m} - \alpha R_{ijk}^{m} \tag{A1}$$

where α is the overrelaxation coefficient and the residual R is given by

$$R_{ijk} = L_D(\psi_{ijk}) - F_{ijk} \tag{A2}$$

L_D is the finite difference operator for the left-hand side of (2) and F is the finite difference value of the right-hand side forcing function. Iteration was continued until the largest residual was less than a specified

value ϵ. The adequacy of the choice for ϵ was checked by computing three ψ fields for three separate forcing functions and insuring that their sum was equal (within truncation error) to ψ computed from the sum of the forcing. When $\epsilon \sim 10^{-2}\bar{\psi}$ (where $\bar{\psi}$ is the average streamfunction value), this latter condition was not met; $\epsilon \sim 10^{-3}\bar{\psi} = 1 \times 10^6$ was required.

Results were insensitive to the value of α, but the number of scans required for convergence varied by more than an order of magnitude between $\alpha = 1.30$ and 1.95, the latter of which was the optimum value.

One difficulty arose due to the relatively coarse vertical resolution in the original ECMWF analyses; 100 and 200 mb levels were available, but not 150 mb. The interpolated $\bar{\theta}$ field for a particular time is shown in Fig. A1. Because the 100 mb level lies in the stratosphere and the 200 mb level in the troposphere, the effective tropopause in the input to Eq. (2) occurred at 200 mb, where a first order discontinuity in $\bar{\theta}$ was present. In reality, the tropopause was closer to 150 mb, at least near the hurricane center, and stability was likely overestimated between 150 and 200 mb in the calculations. No objective solution could be found to this problem. Potential temperature could have been defined at 150 mb using climatological vertical gradients or some more complex procedure, but 150 mb winds would also have had to be redefined. In addition, the calculation region included a low-tropopause middle latitude trough and a high-tropopause tropical storm, and no means of defining 150 mb θ values avoided the need for arbitrary decisions. As a result, the artificially low tropopause was accepted as is. Figure 20 showed that even removing the troposphere–stratosphere distinction by setting stability to a constant produced similar solutions. It is thus unlikely that the lack of 150 mb data seriously compromised the results.

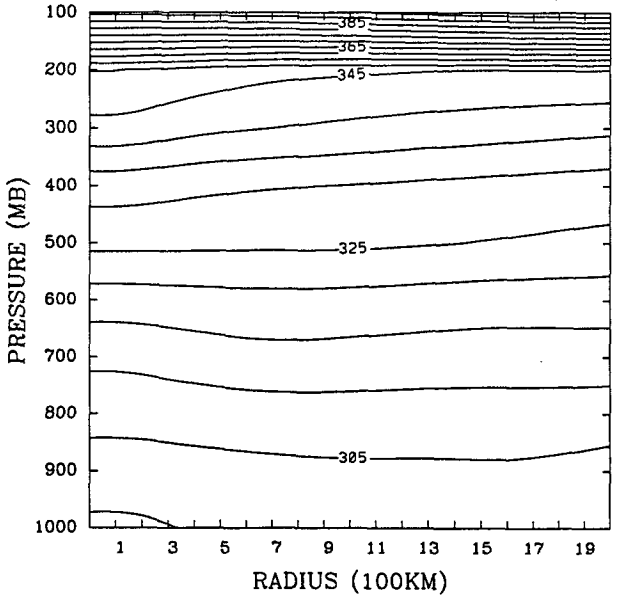

FIG. A1. Radial–vertical cross section of potential temperature at 0000 UTC 31 August. Increment: 5 K.

A second difficulty arose because u' and ω' had to be determined from the imperfect ECMWF radial velocity fields. In principle, it would have been possible to compute the mean radial–vertical circulation induced by the eddy fluxes, then recalculate the eddy fluxes based on the calculated $\bar{u}$ and $\bar{\omega}$ fields, and iterate the process until it converged. This was not done because the calculated mean fields did not include the effects of heating and friction, both of which undoubtedly played a major role in the true mean fields. It was viewed as more realistic to assume that the radial and vertical eddy fluxes were acceptable as analyzed. The implied assumption is that if exact heating and friction contributions had been known, the resulting radial–vertical circulation would have resembled that observed.

Finally, the Coriolis parameter was computed as $2\Omega \sin\phi$, but the nonzero $\bar{f}'$ terms which result (Holland 1983) were neglected. To insure that the large $\overline{f'u'}$ did not arise from this neglect, the Coriolis parameter was recomputed using the local β plane at the storm center at each observation time. The change in the forcing function in (2) arising from the β plane assumption was negligible.

REFERENCES

Betts, A. K., 1986: A new convective adjustment scheme. Part I: Observational and theoretical basis. *Quart. J. Roy. Meteor. Soc.*, **112**, 677–692.

Burpee, R. W., D. G. Marks and R. T. Merrill, 1984: An assessment of omega drop-windsonde data in track forecasts of Hurricane Debby (1982). *Bull. Amer. Meteor. Soc.*, **65**, 1050–1058.

Eliassen, A., 1952: Slow thermally or frictionally controlled meridional circulation in a circular vortex. *Astrophys. Norv.*, **5**, 19–60.

Emanuel, K. A., 1986: An air-sea interaction theory for tropical cyclones. Part I: Steady-state maintenance. *J. Atmos. Sci.*, **43**, 585–604.

Gray, W. M., 1979: Hurricanes: Their formation, structure, and likely role in the tropical circulation. *Meteorology Over the Tropical Oceans*, D. B. Shaw, Ed., Roy. Meteor. Soc., 155–218.

Heckley, W. A., M. J. Miller and A. K. Betts, 1987: An example of hurricane tracking and forecasting with a global analysis-forecasting system. *Bull. Amer. Meteor. Soc.*, **68**, 226–229.

Holland, G. J., 1983: Angular momentum transports in tropical cyclones. *Quart. J. Roy. Meteor. Soc.*, **109**, 187–210.

——, 1988: Mature structure and structure change. *A Global View of Tropical Cyclones*, R. L. Elsberry, Ed., Naval Postgraduate School, 13–52.

——, and R. T. Merrill, 1984: On the dynamics of tropical cyclone structural changes. *Quart. J. Roy. Meteor. Soc.*, **110**, 723–745.

Hollingsworth, A., J. Horn and S. Uppala, 1989: Verification of FGGE assimilations of the tropical wind field: the effect of model and data bias. *Mon. Wea. Rev.*, **117**, 1017–1038.

Hoskins, B. J., M. E. McIntyre and A. W. Robertson, 1985: On the use and significance of isentropic potential vorticity maps. *Quart. J. Roy. Meteor. Soc.*, **111**, 877–946.

Lee, C. S., R. Edson and W. M. Gray, 1989: Some large-scale characteristics associated with tropical cyclone development in the

North Indian Ocean during FGGE. *Mon. Wea. Rev.*, **117**, 407–426.

Lord, S. J., and J. L. Franklin, 1987: The environment of Hurricane Debby (1982). Part I: Winds. *Mon. Wea. Rev.*, **115**, 2760–2780.

McBride, J. L., and R. Zehr, 1981: Observational analysis of tropical cyclone formation. Part II: Comparison of non-developing versus developing systems. *J. Atmos. Sci.*, **38**, 1132–1151.

Merrill, R. T., 1988: Characteristics of upper-tropospheric environmental flow around hurricanes. *J. Atmos. Sci.*, **45**, 1665–1677.

Molinari, J., and S. Skubis, 1985: Evolution of the surface wind field in an intensifying tropical cyclone. *J. Atmos. Sci.*, **42**, 2865–2879.

——, and D. Vollaro, 1989a: External influences on hurricane intensity. Part I: Outflow layer eddy angular momentum fluxes. *J. Atmos. Sci.*, **46**, 1093–1105.

——, and ——, 1989b: Interaction of a hurricane with a baroclinic wave. Preprints, *18th Conf. on Hurricanes and Tropical Meteorology*, San Diego, 50–51. [Available from American Meteorological Society, 45 Beacon St., Boston, MA., 02108.]

Ooyama, K. V., 1982: Conceptual evolution of the theory and modeling of the tropical cyclone. *J. Meteor. Soc. Jpn.*, **60**, 369–379.

——, 1987: Numerical experiments of steady and transient jets with a simple model of the hurricane outflow layer. Preprints, *17th Conf. on Tropical Meteor.*, Miami, 318–320. [Available from American Meteorological Society, 45 Beacon St., Boston, MA., 02108.]

Pfeffer, R. L., and M. Challa, 1981: A numerical study of the role of eddy fluxes of momentum in the development of Atlantic hurricanes. *J. Atmos. Sci.*, **38**, 2393–2398.

Reed, R. J., A. Hollingsworth, W. A. Heckley and F. Delsol, 1988: An evaluation of the performance of the ECMWF operational system in analyzing and forecasting easterly wave disturbances over Africa and the tropical Atlantic. *Mon. Wea. Rev.*, **116**, 824–865.

Rotunno, R., and K. A. Emanuel, 1987: An air–sea interaction theory for tropical cyclones. Part II: Evolutionary study using a nonhydrostatic axisymmetric numerical model. *J. Atmos. Sci.*, **44**, 542–561.

Schubert, W. H., and J. J. Hack, 1982: Inertial stability and tropical cyclone development. *J. Atmos. Sci.*, **39**, 1687–1697.

Shapiro, L. J., and H. E. Willoughby, 1982: The response of balanced hurricanes to local sources of heat and momentum. *J. Atmos. Sci.*, **39**, 378–394.

Skubis, S., and J. Molinari, 1987: Angular momentum variation in a translating cyclone. *Quart. J. Roy. Meteor. Soc.*, **113**, 1041–1048.

Smith, R. K. 1981: The cyclostrophic adjustment of vortices with application to tropical cyclone modification. *J. Atmos. Sci.*, **38**, 2021–2030.

Sundqvist, H., 1970: Numerical simulation of the development of tropical cyclones with a ten-level model. Part I. *Tellus*, **22**, 359–390.

Wergen, W., 1988: The diabatic ECMWF normal mode initialization scheme. *Beitr. Phys. Atmos.*, **61**, 274–302.

Willoughby, H. E., 1988: The dynamics of the tropical cyclone core. *Austr. Meteor. Mag.*, **36**, 183–192.

——, 1989: Temporal changes of the primary circulation in tropical cyclones. *J. Atmos. Sci.*, **47**, 242–264.

——, J. A. Clos and M. G. Shoreibah, 1982: Concentric eye walls, secondary wind maxima, and the evolution of a hurricane vortex. *J. Atmos. Sci.*, **39**, 395–411.

——, H.-L. Jin, S. J. Lord and J. M. Piotrowicz, 1984: Hurricane structure and evolution as simulated by an axisymmetric, nonhydrostatic numerical model. *J. Atmos. Sci.*, **41**, 1169–1186.